PROCEEDINGS OF SPIE

SPIEDigitalLibrary.org/conference-proceedings-of-spie

# Hexagonal boron nitride (h-BN) 2D nanoscale devices for classical and quantum signal transduction

Wang, Yanan, Feng, Philip X.-L.

Yanan Wang, Philip X.-L. Feng, "Hexagonal boron nitride (h-BN) 2D nanoscale devices for classical and quantum signal transduction," Proc. SPIE 11081, Active Photonic Platforms XI, 1108111 (12 September 2019); doi: 10.1117/12.2529858

SPIE.

Event: SPIE Nanoscience + Engineering, 2019, San Diego, California, United States

# Hexagonal boron nitride (h-BN) 2D nanoscale devices for classical and quantum signal transduction

Yanan Wang[1,2*], Philip X.-L. Feng[1,2*]

[1]Electrical and Computer Engineering, Herbert Wertheim College of Engineering, University of Florida, Gainesville, FL 32611, USA
[2]Electrical Engineering, Case School of Engineering, Case Western Reserve University, OH 44106, USA

## ABSTRACT

Hexagonal boron nitride (h-BN) crystals possess ultrawide electronic bandgap of 5.9 eV and excellent chemical and thermal stability. Nanometer-scale thin films and atomic layers derived from the layered bulk of h-BN crystals have been widely adopted for enabling new two-dimensional (2D) devices and systems, thanks to its excellent dielectric, optical, mechanical, and thermal properties. Lately, h-BN thin layers have also emerged as an attractive material and device platform for nanoscale optics, photonics, and quantum engineering. In this proceedings paper, we report on some of our studies and initial results toward developing integrated photonic circuitry based on this van der Waals (vdW) layered crystal. The first part summarizes our effort on the creation and optical characterization of defect-related quantum emission in exfoliated and dry-transferred h-BN flakes. Based on the statistics from our measurements and state-of-the-art knowledge in the field, we have identified a group of emitters with emission wavelength around 710 nm exhibiting large Debye-Waller (DW) factor. We then describe optical waveguide and cavity designs at the wavelength range of interest, with the aim of achieving high optical cooperativity. Combined with our studies in ultrathin h-BN crystalline nanomechanical resonators and phononic waveguides, these new explorations in quantum emitters will help pave the way to facilitating h-BN photonic devices and integrated systems for both classical and quantum applications.

**Keywords:** Hexagonal boron nitride (h-BN), van der Waals crystal, wide-bandgap material, quantum emitter, defect center, single photon source, integrated photonic circuitry, quantum photonics

## 1. INTRODUCTION

Nonclassical light sources such as single photon emitters (SPEs) have attracted extensive attention as critical building blocks for the realization of photonic circuitry, especially towards quantum computing[1], communication[2], and sensing applications[3]. Distinct from thermal light sources (such as incandescent light bulbs) and coherent light sources (such as lasers), an ideal SPE can produce only one photon within its fluorescence lifetime, and all successive photons are indistinguishable with controllable quantum correlations. Optically active defect centers in three-dimensional (3D) wide-bandgap (WBG) crystals, such as diamond and silicon carbide (SiC), have been demonstrated as paradigm sources of quantum emission, due to the unique combination of desirable optical properties with the convenience of operation and potential for scalability[4,5]. Such a defect-related quantum emitter can be considered as an "inverted atom", with one atom removed or replaced in an otherwise perfect crystal lattice. The wide bandgap of the host crystal provides excellent electronic isolation – the optical transitions between discrete defect states are shielded from the influence of electrons in the host crystal's valence and conduction bands. Therefore, these atom-like defect centers can emit robust single photons even at room temperature. Moreover, via spin-photon interactions, the defect centers can facilitate initialization and readout of individual electron spins, along with their proximal nuclear spins, with optical fields.

The existence of such quantum emitters in an emerging two-dimensional (2D) WBG crystal, namely hexagonal boron nitride (h-BN), has been explored since late 2015[6]. h-BN layers isolated from its bulk crystal inherit the ultrawide electronic bandgap (5.9 eV)[7] and excellent chemical and thermal stability. It has conventionally been incorporated into van der Waals (vdW) heterostructures as atomically smooth dielectric layers for enabling high-performance 2D electronic and optoelectronic devices. The outstanding mechanical properties of h-BN, including a theoretical Young's

*Correspondence Emails: yanan.wang@ufl.edu; philip.feng@ufl.edu

Active Photonic Platforms XI, edited by Ganapathi S. Subramania, Stavroula Foteinopoulou,
Proc. of SPIE Vol. 11081, 1108111 · © 2019 SPIE · CCC code: 0277-786X/19/$21
doi: 10.1117/12.2529858

modulus as high as $E_Y \sim 780$ GPa and a breaking strain limit up to ~22%[8], have also been exploited to develop robust resonant nanoelectromechanical systems (NEMS) and multimode nanomechanical flexural resonators with spatially visualized mode shapes[9,10]. There has also been growing research in exploring the exotic optical properties of h-BN, such as the hyperbolic nature and strong phonon polaritons, which may lead to near-field optical imaging, guiding, and focusing functionalities over a broad spectral range in the technologically important infrared (IR) ranges[11].

Over the past three years, preliminary demonstrations of creating and controlling of quantum emitters in h-BN have been accomplished via electron/ion irradiation[12], strain engineering[13], and electrical stark tuning[14]. More intriguingly, magnetic field dependent emission[15] and Rabi oscillation[16] have been reported earlier this year, which suggest the possibilities of spin-related states or triplet states existing in h-BN. Despite the fact that the physical nature of these defect centers is still under investigation, h-BN has been proven to be an attractive and excellent host of quantum emission, with strong zero phonon line (ZPL), high single photon purity even at 800 K, a short radiative lifetime <1 ns, and an exceptional single photon emission rates >$10^6$ counts/s (Ref. 4). The vdW nature of h-BN crystal also endorses unparalleled advantages in heterogeneous integration schemes, free from lattice matching constraints. Further, the planar geometry of h-BN crystal is beneficial for coupling the emission out to optical waveguides, cavities, and plasmonic devices. Taking advantages of these exceptional quantum emission characteristics of h-BN and its potential in optomechanics and IR optics, we envision an integrated photonic platform based on h-BN, and its hybrid with more mature photonic materials and device platforms, as conceptually illustrated in Figure 1.

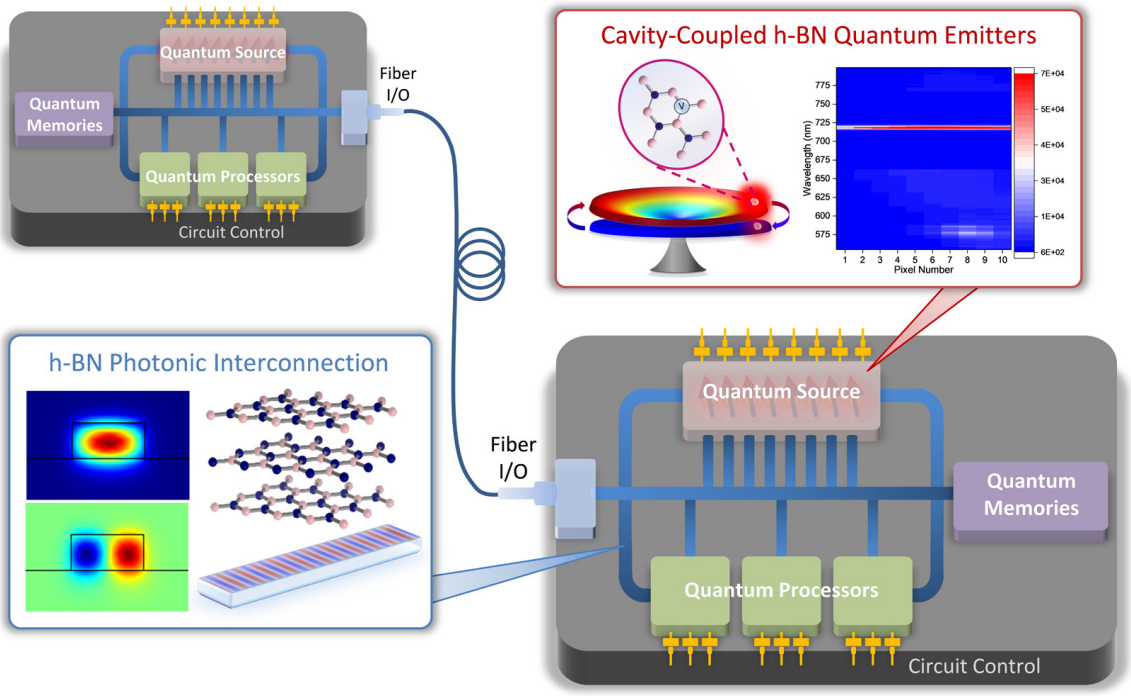


Figure 2. Conceptual illustration of the envisioned hybrid integrated photonic circuitry based on h-BN crystalline devices.

The integrated photonic circuitry we envision here consists of the following main components. The defect centers in h-BN crystals are utilized as single photon sources and will be incorporated into photonic cavities, in order to enable active optomechanical and/or electromechanical control. The photons will be routed through h-BN or hybrid optical waveguides and reach the processing and storage units, which are based on arrays of Mach-Zehnder interferometers and microdisk or microring resonators. The interconnection between different circuit nodes is achieved by wavelength converters and off-chip fibers. Such a photonic integrated circuitry paradigm can serve as a unique testbed for demonstrating functionalities in both classical and quantum regimes. Toward this overarching goal, we have conducted studies on the optical characterization of quantum emission in mechanically exfoliated h-BN crystals, and have performed mode engineering in photonic components based on h-BN, as well as the development of h-BN nanomechanical phononic crystal waveguides[17]. The present work may provide valuable guidelines for designing and optimizing quantum emitters and h-BN photonic devices toward the realization of integrated photonic systems.

## 2. EXPERIMENTAL METHODS

### 2.1 h-BN sample preparation

Hexagonal boron nitride films can be obtained through either epitaxial growth using chemical vapor deposition (CVD) or mechanical exfoliation of flakes from a bulk crystal. In this work, we employ a suite of specially developed, completely dry exfoliation and transfer techniques as illustrated and detailed in our previous works[17,18,19]. h-BN flakes are mechanically isolated from a high-quality bulk h-BN crystal and pressed onto polydimethylsiloxane (PDMS) stamps. After exfoliation, the multilayer h-BN sheets with lateral size from tens to hundreds of micrometers are transferred onto patterned silicon dioxide on silicon (290-nm $SiO_2$/Si). As-prepared samples consist of both supported and suspended h-BN regions, serving as ideal platforms for exploring the influence of dielectric environment on the light coupling and optical contrast of h-BN. Prior to the optical characterization, high-temperature annealing at 850 °C under 1 Torr of nitrogen is performed, to activate the defect centers and to desorb any possible surface contaminants.

### 2.2 Focused ion beam (FIB) patterning

In order to intentionally create or activate defect centers in h-BN, we selectively pattern h-BN using a gallium (Ga) focused ion beam (FIB). Square-shaped patterns are defined on mechanical exfoliated h-BN flakes using an FEI Nova NanoLab 200 field emission gun (FEG) system, which combines high-resolution field emission scanning electron microscopy (SEM) for microanalysis and a FIB for precise etching. The $Ga^+$ ion current and voltage are set as 100 pA and 30 kV, respectively, and the exposure time and total dosage are controlled by the etching depth varied from 2 nm to 10 nm. Additional high-temperature annealing at 850 °C may be performed to remove possible carbon residues deposited during FIB etching. The effects of FIB patterning will be further discussed in Sub-Section 3.3.

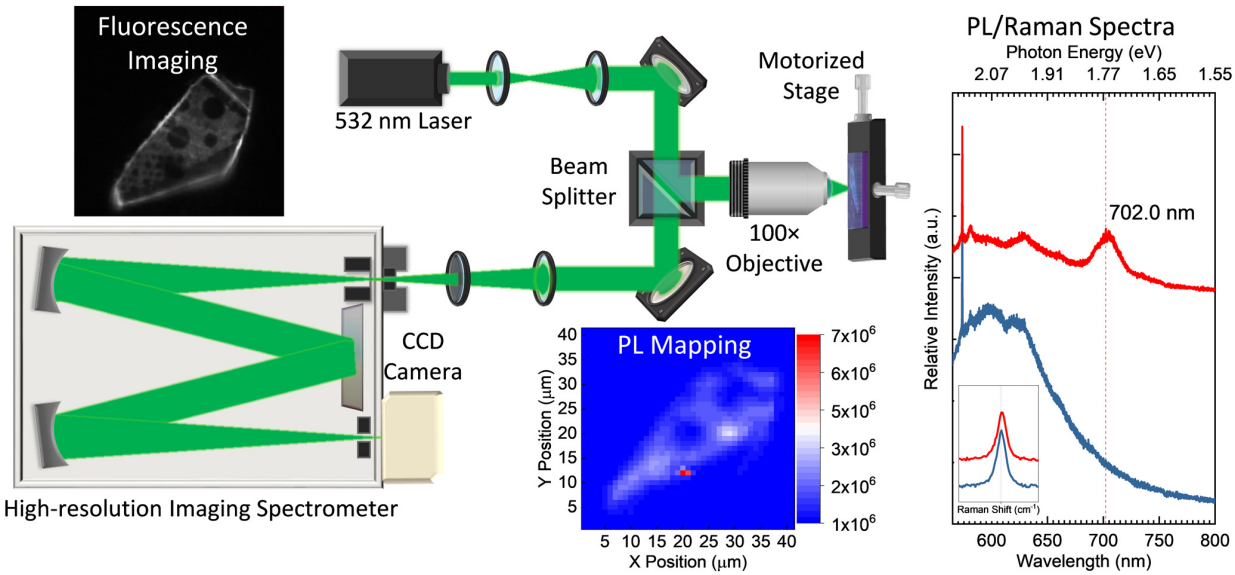


Figure 2. Schematic illustration of the optical spectroscopy system. The emission is excited by a 532-nm continuous wave (CW) laser with laser power below 1 mW and then collected via a 100× objective. The fluorescence images and photoluminescence (PL) spectra over a wide spectral range are recorded by a Princeton Instruments 2500 spectroscopic system, while the PL mapping results are performed in a different system equipped with a Horiba iHR550 spectrometer.

### 2.3 Optical characterization

To better understand the crystal quality and defect behaviors in these h-BN samples, we use spectroscopic tools to probe the vibrational modes and photoluminescence (PL) in the materials. Our system consists of a green laser (532 nm), high-magnification optical objectives (50× or 100×), and a spectrometer (Horiba iHR550 or Princeton Instruments 2500) with a detector sufficiently sensitive to record the weak scattered light signals for Raman and single photon measurement (Figure 2). The customized microscopy system based on a Princeton Instruments 2500 contains of a back-illuminated electron-multiplying charge-coupled device (CCD) and can be utilized to capture fluorescence images with a divergent incident laser beam. While the other system equipped with a Horiba iHR550 is capable of acquiring detailed and local

information with a high spatial resolution (~1 μm) and spectral resolution (~0.30 nm). Facilitated by a motorized stage, it can reveal both PL and Raman mapping over a certain spatial range. Correlation measurements are performed by using the Hanbury Brown and Twiss (HBT) interferometry techniques at zero delay time, to further verify the single photon nature of the emission process. Without specification, all the measurements are conducted at room temperature. The optical characterization results are presented and further elaborated in the following Section 3.

## 3. OPTICAL CHARACTERIZATION OF QUANTUM EMITTERS

### 3.1 Basic properties and defect states in h-BN

Because of the ultrawide bandgap, h-BN bulk crystal exhibits limited absorption to the visible light and thereby appears transparent in the visible range (Figure 3a). When the flakes are exfoliated and isolated from the bulk crystal, they may appear colorful dependent on the interferometry conditions formed inside the h-BN flakes and with their dielectric surroundings. Based on our previous study[19] on optical contrast of h-BN, the interference from h-BN itself starts to play a role as the number of layers exceeds ~300, which corresponds to a thickness of ~100 nm. To identify h-BN flakes with smaller thickness (< 100 nm), such as the one shown in Figure 2b, a cavity formed between the h-BN crystal and the underlying dielectric layer would be helpful. Therefore, oxidized silicon (290-nm $SiO_2$/Si) substrate are preferred over bare Si to better visualize the thin layers of crystalline h-BN.

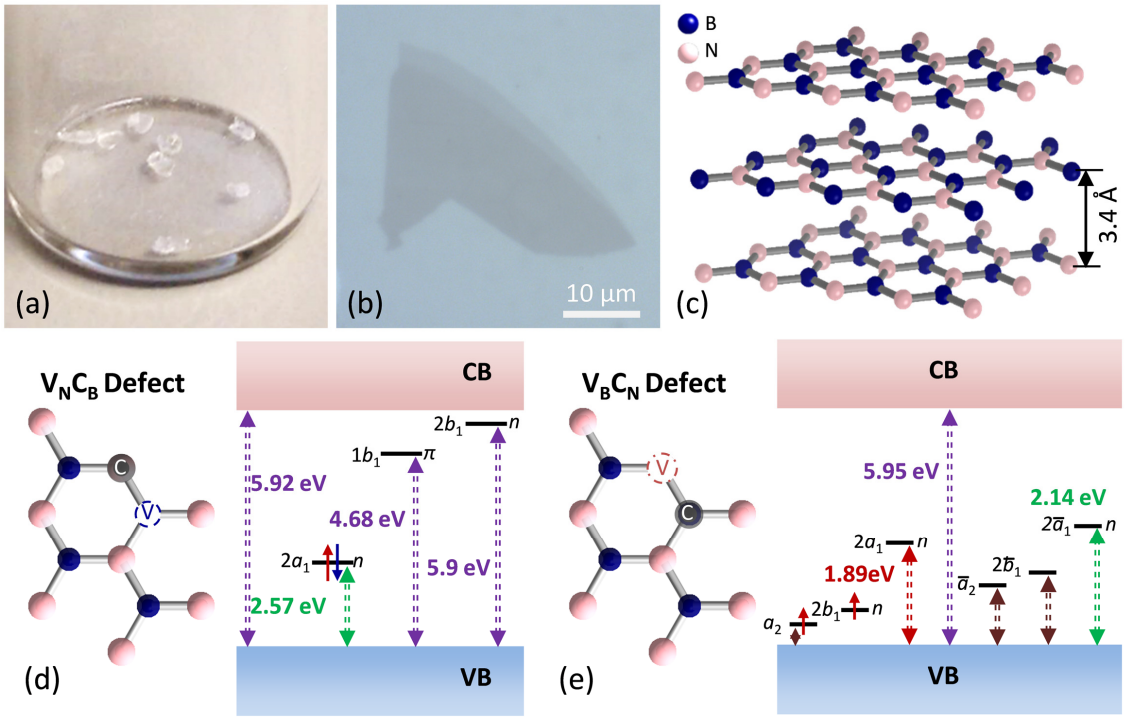


Figure 3. (a) A typical optical image of h-BN crystals. (b) A representative optical microscopy image of mechanically exfoliated h-BN on bare Si substrate. (c) Schematic illustration of layered crystal structure of h-BN. Possible defect sites of (d) $V_NC_B$ and (e) $V_BC_N$ in h-BN and their corresponding defect state energy diagrams[20].

According to *ab initio* calculations conducted in Ref. 20, there are a number of possible defect centers that can be promising candidates for quantum applications. As presented in Figure 3d-3e, different defect sites will give rise to distinctive energy states. It needs to point out that even for one specific type of defect, there are multiple allowed optical transitions, which lead to variation in the ZPL positions observed experimentally.

### 3.2 Spectral characteristics of quantum emission in h-BN

We have studied tens of h-BN flakes dry-transferred onto various structures patterned on $SiO_2$/Si substrates. Typical fluorescence images, PL mapping results, and spectra of emission in h-BN flakes are summarized in Figure 2 and Figure 4. Flakes in Figure 4a and 4c are transferred onto arrays of microtrenches patterned $SiO_2$/Si substrates; therefore,

portions of the flakes are suspended over circular microtrenches or cavities. The flake in Figure 4e is fully supported by $SiO_2$/Si substrate. From the fluorescence images, we can directly observe that strong emission inclines to occur at the edges or steps of the flakes, probably due to higher defect density at those locations. However, most bright locations exhibit broad emission spectra as shown in Figure 4h, suggesting that these areas may be overly defective, and thus clusters of emitters form. Relatively more isolated bright spots in the fluorescence image, as labeled in Figure 4e, have a higher chance to contain single emitters. As illustrated in the pixel image (Figure 4f) and the spectral plot (red curve in Figure 4i), the emission from measurement spot labeled in the red circle has a narrow spectral linewidth of ~17 nm. The photon purity of this spot is further characterized by the HBT correlation measurement. Correlation curve (Figure 4g) of measured $g^2(\tau)$ with a dip approaching 0.5 at $\tau$=0 implies the existence of a single photon emitter or an ensemble of two.

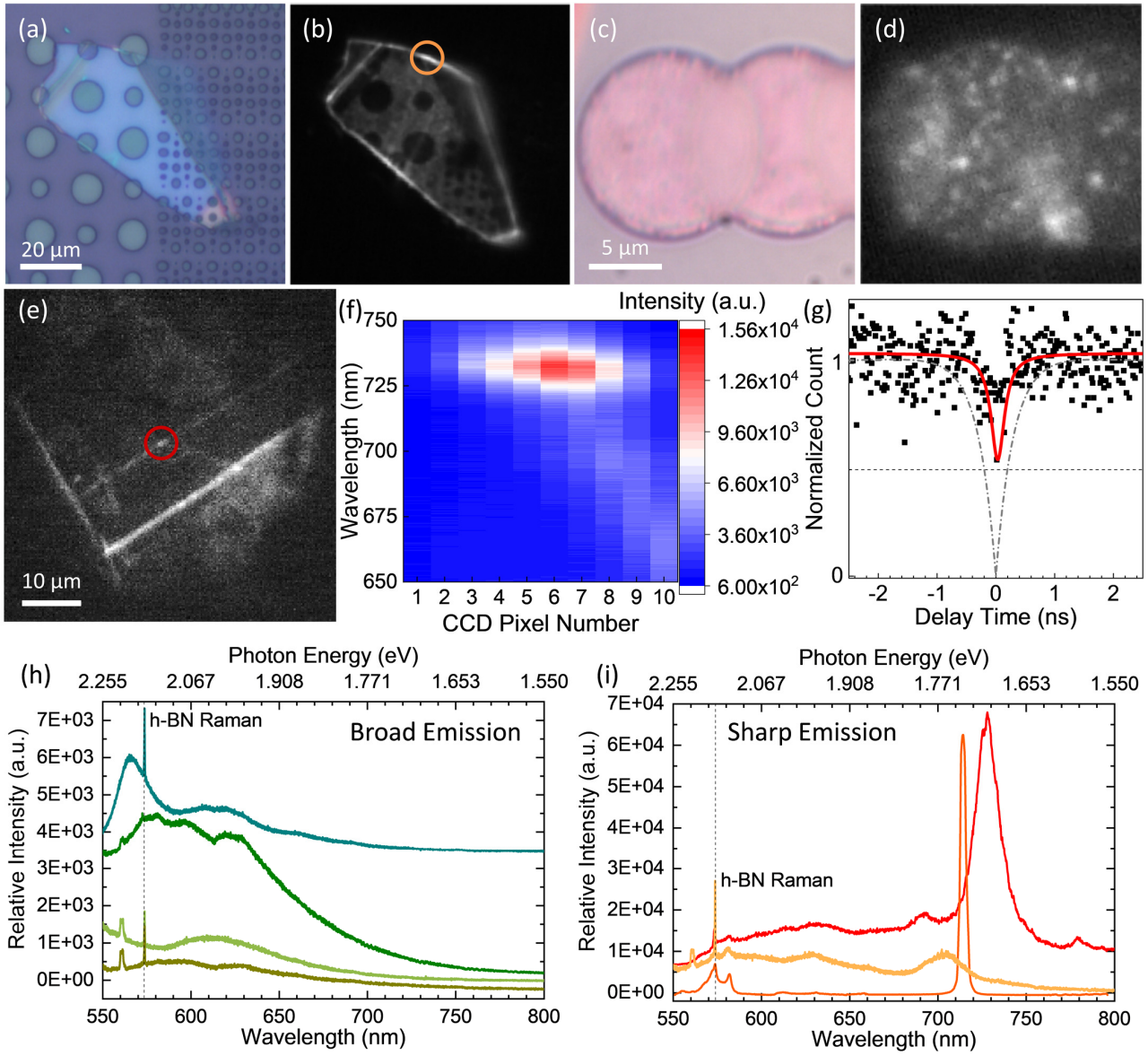


Figure 4. (a) & (c) Typical optical microscopy images of h-BN flakes on patterned $SiO_2$/Si substrates. (b), (d) & (e) Fluorescence images of h-BN flakes under unfocused 532-nm laser excitation. (f) & (g) Pixel image and correlation measurement $g^2(\tau)$ curve of measurement spot labeled by the red circle in (e). (h) & (i) Representative PL spectra of two groups of defect emission. The yellow and red curves in (i) are taken from the spots labeled in (b) and (e), respectively.

From the above discussion, we can generally divide the emitters into two categories by the linewidth of emission, as summarized in Figure 4h-4i. Interestingly, most of the sharp emission lines in our measurements appear at the wavelength around 710 nm. At room temperature, a linewidth as small as ~3.2 nm has been observed with a central peak wavelength at 714 nm. This agrees well with the observations in Ref. 12. They ascribe the two groups likely corresponding to two similar defects but in different local dielectric environment.

### 3.3 Influence of FIB patterning

The emitters discussed above originate from unintentionally formed crystal defects in h-BN crystals. In order to gain more control over the formation or activation of defect centers in h-BN, we investigate the influence of FIB patterning. As illustrated in Figure 5a, an exfoliated h-BN flake is milled with square-shaped patterns by FIB, and the depth of patterns is varied from 2 nm to 10 nm. However, the patterned areas do not readily show obvious contrast from the pristine parts under the fluorescence imaging. PL spectra from spot measurements are summarized in Figure 5c; and broad emission background can be observed for all the cases. The emerging features around the h-BN Raman peak may be related to the broadening of h-BN transverse optical (TO) mode and G peak of C-C bond, suggesting as-treated h-BN is probably too defective to host isolated SPEs. It is worth mentioning that the PL measurements are performed after additional high-temperature annealing (at 850 °C) with the aim of removing possible carbon deposition during the FIB etching process, while it appears still not efficient to remove the broad background emission. We note that similar observations on such FIB patterning effects have been recently reported in Ref. 21.

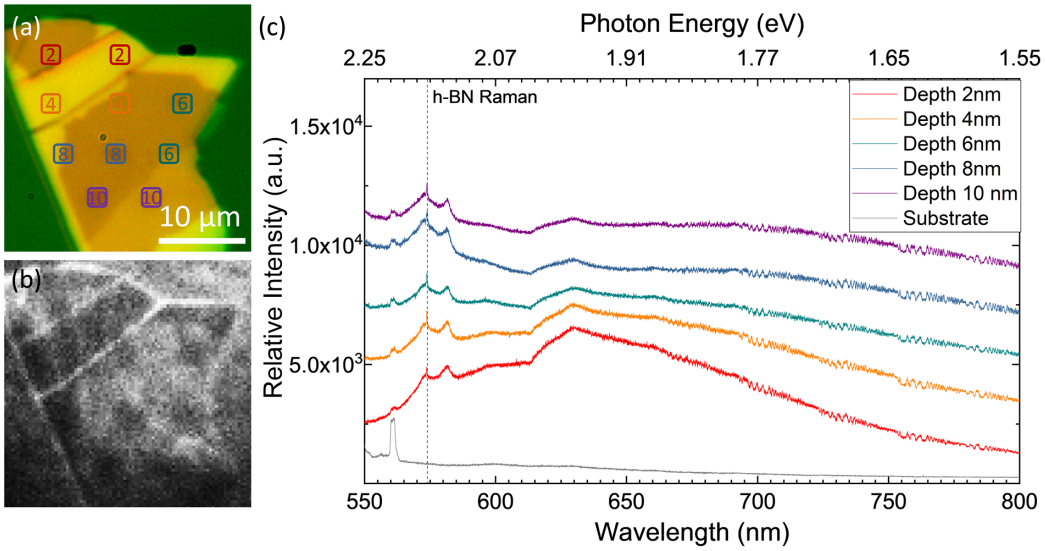


Figure 5. (a) & (b) Optical microscopy image and fluorescence image of an h-BN flake milled with square-shaped patterns with depth varying from 2 nm to 10 nm. (c) Corresponding PL spectra measured after additional high-temperature annealing (at 850 °C) of the h-BN sample.

### 3.4 Comparison with state-of-the-art quantum emitters

Based on our measurements and literature survey, we summarize the key characteristics of quantum emitters in h-BN and make comparison with the state-of-the-art emitters in 3D WBG crystals, diamond and SiC, as presented in Table 1. With maximum count rate up to $10^7$ counts/s, quantum emitters in h-BN are among the brightest SPEs at room temperature. Also, emitters in h-BN exhibit much narrower spectral linewidth at room temperature compared to the nitrogen vacancies in diamond and silicon vacancies in SiC. For an ideal SPE, the linewidth should be determined by the emission lifetime and narrower linewidth means a higher chance to emit indistinguishable photons. The coupling strength between the defect emission and the optical cavity is described as optical cooperativity,

$$C = \frac{3}{4\pi^2}\left(\frac{\lambda}{n_0}\right)^3 \frac{Q}{V}\frac{\gamma_{zpl}}{\gamma_{total}}\left|\frac{\vec{E}(\vec{r}_d)}{\vec{E}(\vec{r}_m)}\right|^2, \quad (1)$$

where λ is the ZPL wavelength, $n_0$ is the effective index of the cavity, $Q$ is the quality factor, $V$ is the mode volume, $\gamma_{ZPL}$ and $\gamma_{total}$ are the rate of ZPL emission and the total rate of spontaneous emission, respectively, $\vec{E}(\vec{r}_d)$ and $\vec{E}(\vec{r}_m)$ represent the electric fields where the defect center and the maximum electric field of cavity are located[22]. From the above equation, we can see the coupling strength is directly proportional to the emission fraction into the ZPL, or so-called Debye-Waller (DW) factor. SPEs in h-BN possess a DW factor as high as 0.82, superior to their counterparts in 3D WBG crystals, which means it is likely to achieve strong coupling between SPEs in h-BN and optical cavities.

Table 1. Comparison of state-of-the-art quantum emitters. All specs are collected from measurements at room temperature.

| | Emission wavelength (nm) | Maximum count rate (counts/s) | Spectral linewidth (nm) | Emission lifetime (ns) | Emission fraction into ZPL | Spectral / spatial controllability | Integration possibility |
|---|---|---|---|---|---|---|---|
| **Diamond** | NV: 575 nm<br>$NV^-$: 635 nm<br>SiV: 738 nm | NV: ~$10^6$<br>$NV^-$: ~$10^3$<br>SiV: ~$10^6$ | $NV^-$: >100 nm<br>SiV: ~ 4 nm | NV: 12–22<br>SiV: ~1 | NV: ~0.03<br>$NV^-$: ~0.03<br>SiV: > 0.7 | Yes, comparatively more control | Yes |
| **SiC** | DV: 1133–1127 nm<br>$V_{Si}^-$: 885 nm | ~$10^6$ | DV: ~2 nm<br>$V_{Si}^-$: > 100 nm | DV: ~10<br>$V_{Si}^-$: ~10 | DV: ~0.07<br>$V_{Si}^-$: ~0.4 | Yes, but not deterministic yet | Yes |
| **h-BN (Monolayers to bulk crystals)** | Multiple sharp lines over a wide spectral range (570–820 nm) | **~$10^7$** | **1–10 nm** | 1–4 | **0.82** | Yes, but not deterministic yet | Yes |

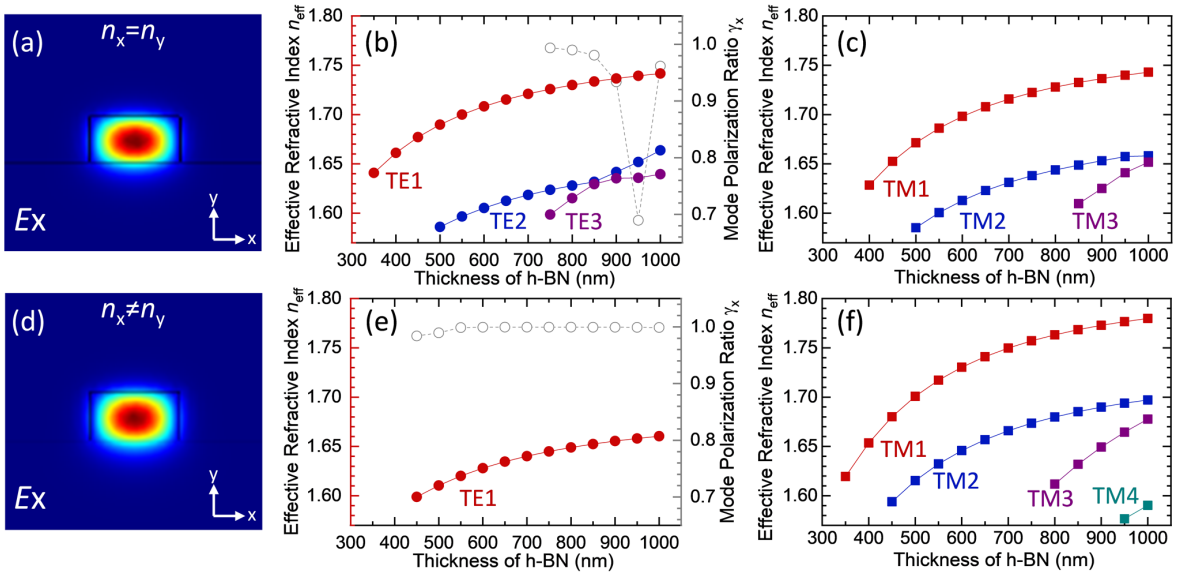


Figure 6. Simulation of effective refractive index and representative mode shapes at a working wavelength of 714 nm for a 1μm-wide h-BN ridge waveguide on bulk $SiO_2$ with varied thickness, by assuming (a) & (c) a normal refractive index of 1.8 and (d) & (e) birefringence indices of 1.72 and 1.84, respectively.

## 4. PHOTONIC COMPONENTS DESIGN

### 4.1 Optical confinement in h-BN

To realize functional devices based on SPEs, it essentially relies on the development of light-matter quantum interface and integration of SPEs with other nanophotonic components. Here, we first investigate the optical confinement in h-BN with a single ridge geometry (Figure 6). As discussed previously, when the number of layers exceeds ~300

(thickness greater than ~100 nm), the interference between the top and bottom surfaces of h-BN starts to play a role in optical contrast. To accurately determine the cut-off thickness, we perform finite element method (FEM) simulations (via COMSOL Multiphysics) with consideration of optical birefringence in h-BN. Figure 6 shows the calculated effective indices for the guided modes supported in a h-BN ridge waveguide sitting on a thick $SiO_2$ layer, with a fixed ridge width of 1 μm and varied thickness from 350 nm to 1000 nm.

To support the quantum emission from h-BN, a target wavelength of 714 nm is set, aligning with the sharp ZPL demonstrated above in Figure 4. Panels (a) to (c) of Figure 6 are attained by assuming h-BN as an optically homogeneous medium with a normal refractive index of 1.8; while panels (d) to (e) are calculated based on setting the ordinary and extraordinary indices as 1.72 and 1.84, respectively. Typically, TE and TM modes propagate with different propagation constants and have different cut-off conditions. The asymmetric boundaries at the top (air) and bottom ($SiO_2$) surfaces lead to a relatively sizeable cut-off thickness excessing 350 nm for all the cases studied in Figure 6. Especially for the TE mode of the birefringent case, due to the relatively smaller ordinary index of 1.74 in the *x*-direction, the cut-off thickness is above 450 nm. For a homogeneous waveguide, mode hybridization and conversion can be observed when the thickness approaches 900 nm (Figure 6b-6c). Such effects are absent from the birefringence case within the studied thickness range, and the mode polarization ratio ($E_x/E_y$) for TE1 mode is close to 100%, suggesting the light can be well confined in an h-BN waveguide.

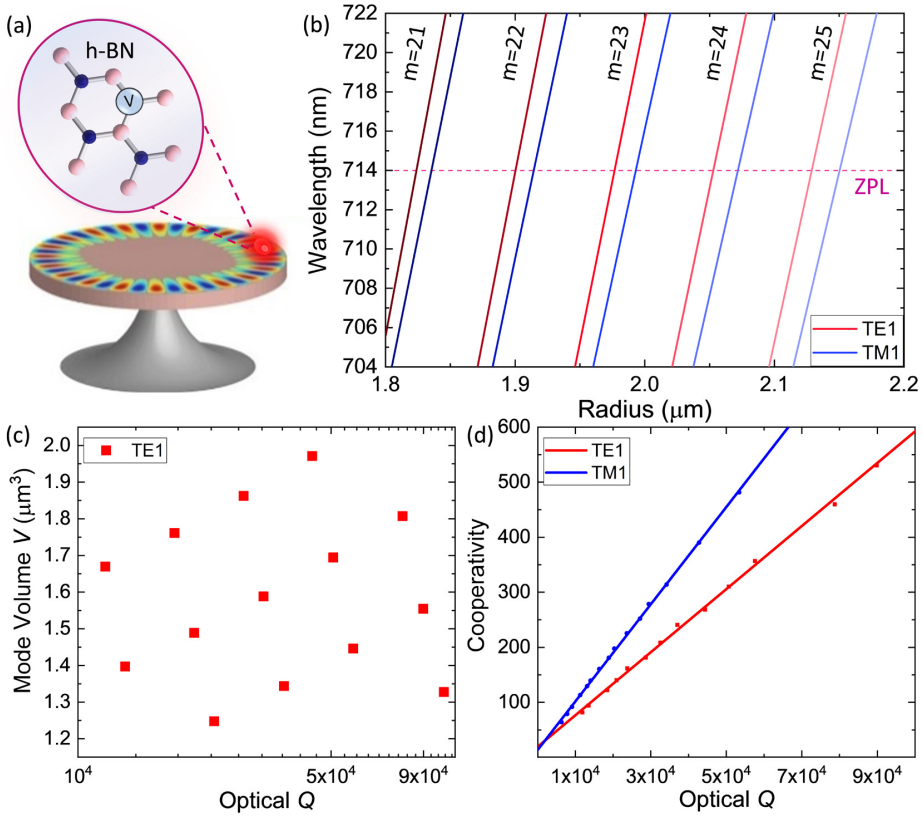


Figure 7. (a) Proposed coupling scheme of quantum emitter and whispering gallery cavity made in h-BN crystal. (b) FEM simulated cavity resonances as a function of disk radius, for cavity modes with azimuthal mode number of 21, 22, 23, 24, 25 in both quasi-TE-like and quasi-TM-like polarizations. The dashed line indicates the wavelength corresponding to the ZPL of the quantum emission in h-BN. (c) & (d) Quality (*Q*) factor, mode volume (*V*) and cooperativity (*C*) extracted from the simulation results in (b) for different cavity modes.

### 4.2 Optical cavity design based on h-BN crystal

In this Sub-Section, we further propose and engineer a whispering gallery optical cavity based on h-BN crystal. SPEs can be coupled to optical cavities using two general approaches, depending on whether the cavities are made from the

same material as the SPE host or not. Here, we are interested in h-BN optical cavities, because this monolithic approach is able to maximize the field overlap between the quantum emitters and the cavity modes. As shown in Equation (1), large overlapping will further enhance the coupling strength between the emitter and the cavity.

A circular microdisk whispering gallery cavity is chosen to overcome the challenge of matching the cavity resonance with the ZPL of quantum emission. The whispering gallery geometry can support many cavity resonances of different azimuthal mode numbers within each mode family[22]. The cavity resonance frequencies can also be flexibly engineered by finely tuning the device radius, as shown in Figure 7. As discussed above, the DW factor of quantum emitters in h-BN can be as high as 0.82. FEM simulations show that an h-BN microdisk with a radius of 2.15 μm and a thickness of 400 nm is able to strongly confine the TE1 optical mode at 714 nm with an effective mode volume less than 1.4 $\mu m^3$, while simultaneously maintaining a radiation-limited optical $Q$ over $10^5$. The estimated Purcell factor of this microdisk resonator is over 750, more significant than the value of 110 predicted for a one-dimension beam cavity design[23]. With these parameters for the whispering gallery cavity design, cooperativity above 500 can be derived, suggesting that h-BN microdisks or microrings are of great promise for realizing strong coherent interactions between the defect centers and the optical cavity, with monolithic integration.

## 5. CONCLUSIONS

In summary, we have investigated the optical properties of novel room-temperature SPEs in h-BN crystal and identified the comparative advantages of h-BN quantum emitters, such as narrow spectral linewidth and significantly large Debye-Waller factor, over their counterparts hosted in conventional 3D WBG crystals such as diamond and SiC. Aiming at exploring and investigating the light-matter interactions, and facilitating development of new devices based on h-BN SPEs, we have evaluated the optical confinement of h-BN ridge waveguides, and further conducted mode engineering of an h-BN whispering gallery optical cavity. Our preliminary numerical analysis shows that microdisk and microring designs possess great potential to achieve substantial Purcell enhancement and strong coupling strength between the SPEs and optical cavity. These initial studies will serve as the stepping stones toward the realization of integrated photonic circuitry based on h-BN crystal and its hybrid with more mature photonic materials, and thus render a broad range of device functionalities for computing, communication, and sensing, in both classical and quantum regimes.

## ACKNOWLEDGEMENTS

The authors are thankful for the financial support from the National Science Foundation (NSF) via the EFRI ACQUIRE program (Grant: EFMA #1641099) and its Supplemental Funding through the Research Experience and Mentoring (REM) program. P.F. also thanks the support from the NSF CAREER program (Grant: ECCS #1454570). We thank J. Berezovsky, J. Lee, V. Zhou, and X.-Q. Zheng for helpful discussions and technical support.

## REFERENCES

[1] Knill, E., Laflamme, R. and Milburn, G. J., "A scheme for efficient quantum computation with linear optics", Nature 409 (6816), 46-52 (2001).
[2] Gisin, N., Ribordy, G., Tittel, W. and Zbinden, H., "Quantum cryptography", Rev. Mod. Phys. 74 (1), 145-195 (2002).
[3] Maze, J. R., Stanwix, P. L., Hodges, J. S., Hong, S., Taylor, J. M., Cappellaro, P., Jiang, L., Dutt, M.G., Togan, E., Zibrov, A.S. and Yacoby, A., "Nanoscale magnetic sensing with an individual electronic spin in diamond", Nature 455 (7213), 644-647 (2008).
[4] Aharonovich, I., Englund, D. and Toth, M., "Solid-state single-photon emitters", Nat. Photonics 10 (10), 631-641 (2016).

[5] Atatüre, M., Englund, D., Vamivakas, N., Lee, S. Y. and Wrachtrup, J., "Material platforms for spin-based photonic quantum technologies", Nat. Rev. Mater. 3 (5), 38-51 (2018).
[6] Tran, T. T., Bray, K., Ford, M. J., Toth, M. and Aharonovich, I., "Quantum emission from hexagonal boron nitride monolayers", Nat. Nanotechnol. 11 (1), 37-41 (2016).
[7] Kubota, Y., Watanabe, K., Tsuda, O. and Taniguchi, T., "Deep ultraviolet light-emitting hexagonal boron nitride synthesized at atmospheric pressure", Science 317 (5840), 932-934 (2007).
[8] Song, L., Ci, L., Lu, H., Sorokin, P. B., Jin, C., Ni, J., Kvashnin, A. G., Kvashnin, D. G., Lou, J., Yakobson, B. I. and Ajayan, P. M., "Large scale growth and characterization of atomic hexagonal boron nitride layers", Nano Lett. 10 (8), 3209-3215 (2010).
[9] Zheng, X.-Q., Lee, J. and Feng, P. X.-L., "Hexagonal boron nitride (h-BN) nanomechanical resonators with temperature-dependent multimode operations", Digest of Tech. Papers, The 18th Int. Conf. on Solid-State Sensors, Actuators & Microsystems (Transducers'15), 1393-1396, Anchorage, Alaska, USA, June 21-25 (2015).
[10] Zheng, X.-Q., Lee, J. and Feng, P. X.-L., "Hexagonal boron nitride nanomechanical resonators with spatially visualized motion", Microsyst. Nanoeng. 3, 17038 (2017).
[11] Dai, S., Fei, Z., Ma, Q., Rodin, A. S., Wagner, M., McLeod, A. S., Liu, M. K., Gannett, W., Regan, W., Watanabe, K. and Taniguchi, T., "Tunable phonon polaritons in atomically thin van der Waals crystals of boron nitride", Science 343 (6175), 1125-1129 (2014).
[12] Tran, T. T., Elbadawi, C., Totonjian, D., Lobo, C. J., Grosso, G., Moon, H., Englund, D. R., Ford, M. J., Aharonovich, I. and Toth, M., "Robust multicolor single photon emission from point defects in hexagonal boron nitride", ACS Nano 10 (8), 7331-7338 (2016).
[13] Grosso, G., Moon, H., Lienhard, B., Ali, S., Efetov, D. K., Furchi, M. M., Jarillo-Herrero, P., Ford, M. J., Aharonovich, I. and Englund, D., "Tunable and high-purity room temperature single-photon emission from atomic defects in hexagonal boron nitride", Nat. Commun. 8 (1), 705 (2017).
[14] Noh, G., Choi, D., Kim, J. H., Im, D. G., Kim, Y. H., Seo, H. and Lee, J., "Stark tuning of single-photon emitters in hexagonal boron nitride", Nano Lett. 18 (8), 4710-4715 (2018).
[15] Exarhos, A. L., Hopper, D. A., Patel, R. N., Doherty, M. W. and Bassett, L. C., "Magnetic-field-dependent quantum emission in hexagonal boron nitride at room temperature", Nat. Commun. 10 (1), 222 (2019).
[16] Konthasinghe, K., Chakraborty, C., Mathur, N., Qiu, L., Mukherjee, A., Fuchs, G. D. and Vamivakas, A. N., "Rabi oscillations and resonance fluorescence from a single hexagonal boron nitride quantum emitter", Optica 6 (5), 542-548 (2019).
[17] Wang, Y., Lee, J., Xie, Y., Zheng, X.-Q. and Feng, P. X.-L., "High-frequency hexagonal boron nitride (h-BN) phononic waveguides", Proc. of The 32nd IEEE Int. Conf. on Micro Electro Mechanical Systems (MEMS'19), 319-322, Coex, Seoul, Korea, January 27-31 (2019).
[18] Yang, R., Zheng, X.-Q., Wang, Z., Miller, C. J. and Feng, P. X.-L., "Multilayer $MoS_2$ transistors enabled by a facile dry-transfer technique and thermal annealing", J. Vac. Sci. Technol. B 32 (6), 061203 (2014).
[19] Wang, Y., Zhou, V., Xie, Y., Zheng, X.-Q. and Feng, P. X.-L., "Optical contrast signatures of hexagonal boron nitride on a device platform", Opt. Mater. Exp. 9 (3), 1223-1232 (2019).
[20] Sajid, A., Reimers, J. R. and Ford, M. J., "Defect states in hexagonal boron nitride: Assignments of observed properties and prediction of properties relevant to quantum computation", Phys. Rev. B 97 (6), 064101 (2018).
[21] Ziegler, J., Klaiss, R., Blaikie, A., Miller, D., Horowitz, V. R. and Alemán, B. J., "Deterministic quantum emitter formation in hexagonal boron nitride via controlled edge creation", Nano Lett. 19 (3), 2121-2127 (2019).
[22] Lu, X., Lee, J. Y., Feng, P. X.-L. and Lin, Q., "High *Q* silicon carbide microdisk resonator", Appl. Phys. Lett. 104 (18), 181103 (2014).
[23] Kim, S., Fröch, J. E., Christian, J., Straw, M., Bishop, J., Totonjian, D., Watanabe, K., Taniguchi, T., Toth, M. and Aharonovich, I., "Photonic crystal cavities from hexagonal boron nitride", Nat. Commun. 9 (1), 2623 (2018).